Proceedings of the Seventeenth International Conference on
Civil, Structural and Environmental Engineering Computing
Edited by: P. Iványi, J. Kruis and B.H.V. Topping
Civil-Comp Conferences, Volume 6, Paper 3.1
Civil-Comp Press, Edinburgh, United Kingdom, 2023
doi: 10.4203/ccc.6.3.1

Seismic Analysis of Twin Tunnels Situated in Liquefiable Grounds using the Domain Reduction Method

Z.X. Fan[1], Y. Yuan[1,2] and Y.S. Yang[3]

[1] Department of Geotechnical Engineering, Tongji University, Shanghai, China
[2]State Key Laboratory of Disaster Reduction in Civil Engineering, Tongji University, Shanghai, China
[3]Shanghai Construction No.4 (Group) Co., Ltd., China

Abstract

This paper presents a novel numerical approach based on the domain reduction method (DRM) for the dynamic analysis of twin tunnels constructed in liquefiable double-layered grounds during earthquakes. The proposed method extends the DRM scheme into saturated layered fields, allowing for accurate reproduction of the seismic wavefield within a non-linear liquefiable subdomain. This novel approach is employed to conduct a parametric analysis of the internal force responses of tunnel linings, investigating the influence of the stiffness ratio of neighboring soil layers, the spacing-radius ratio of twin tunnels, and the angle of incident seismic waves. The results indicate that all three parameters have nonnegligible influences on the tunnel's maximum internal forces.

Keywords: earthquake, liquefaction, domain reduction method, finite element method, layered grounds, twin tunnels

1 Introduction

During strong earthquakes, underground structures located in liquefiable fields are at a greater risk of severe damage [1]. Extensive research has been conducted to study

the dynamic responses of underground tunnels in liquefiable grounds, utilizing model tests [2], analytical methods [3], and numerical methods [4]. However, most of the previous research has focused on water-soil-structure interactions for single-tunnel scenarios. With the increasing development of underground transformational systems in urban areas, many tunnels are now constructed in close proximity to one another, rendering the single-tunnel model unrealistic. In recent years, researchers have conducted simulations to investigate the seismic responses of twin tunnels within liquefiable fields [5]–[7], exploring the effects of tunnel spacing, layout, buried depth, and different seismic inputs. The findings indicate that twin tunnel interaction during liquefaction is significant. Nevertheless, the primary focus of these numerical simulations has been on the structural uplifting and ground responses in proximity, with limited attention paid to the structural internal force responses and only vertically propagating seismic waves considered.

The consideration of boundary effects is crucial in numerical simulations of nonlinear water-soil-structure problems. Many researchers have employed artificial boundary conditions (ABCs) in their numerical models, introducing seismic loadings by applying equivalent forces to boundary nodes [8]. However, most of the current ABCs are designed for internal-source problems and may not perform well in external-source problems. In comparison, the domain reduction method (DRM) is a more sophisticated technique for analyzing seismic-related problems, especially when dealing with inclinedly incident earthquake loadings. Initially proposed by Bielak [9] for topographic effects in seismology, the DRM has been successfully applied to simulate seismic behavior in engineering structures, such as nuclear power plants [10], soil retaining systems [11], and underground structures [12]. To the best of our knowledge, no previous studies have utilized DRM-based methods in the analysis of SSI problems in saturated liquefiable fields.

The primary objective of this study is to develop a DRM-based approach for seismic analysis of underground twin tunnels that considers the inclination of incident earthquake waves and the elastoplastic behavior of soils. To achieve this, a DRM framework for two-phase saturated media will be derived and used to investigate the dynamic responses of twin tunnels located in nonlinear liquefiable layered grounds. The focus of the study will be on the internal force responses of the structures. A parametric analysis will be conducted to thoroughly investigate the influence of the inclined angle of seismic waves, tunnel spacing, and stiffness ratio of neighboring soil layers.

2 Methods

As illustrated in Figure 1, The numerical model has an outer boundary $\hat{\Gamma}^{+}$ that truncates the infinite domain. The model is then further divided into the interior domain Ω^{-} and the auxiliary exterior domain Ω^{+} by the boundaries Γ and Γ_{e}, between which a single-element thick layer is defined. Nodal forces are applied to these boundaries to reconstruct the seismic wavefield in the interior domain. The

region outside the boundary Γ_e serves to dissipate any waves outgoing from the interior domain, ensuring accurate seismic simulations.

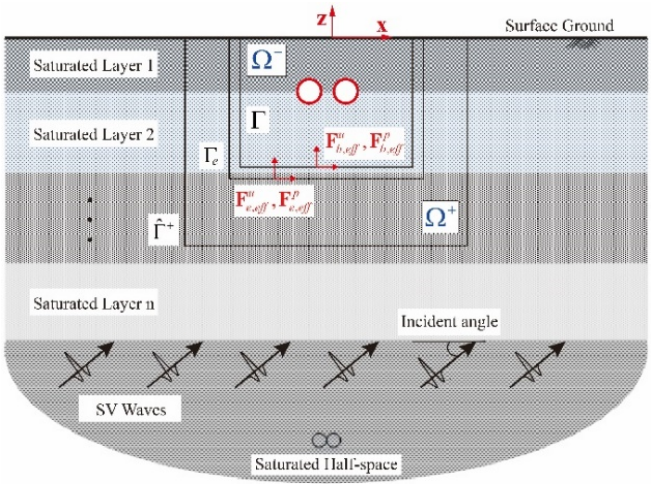

Figure 1: DRM for the SSI problem in layered saturated grounds

The ***u-p*** formulated Biot's equations are chosen for the two-phase media, which can be written in the matrix form as [13]:

$$\boldsymbol{M}\ddot{\boldsymbol{u}} - \boldsymbol{Q}\boldsymbol{p} + \boldsymbol{K}\boldsymbol{u} = \boldsymbol{F}^{\mathrm{u}} \tag{1}$$

$$\boldsymbol{S}\dot{\boldsymbol{p}} + \boldsymbol{Q}^{\mathrm{T}}\dot{\boldsymbol{u}} + \boldsymbol{H}\boldsymbol{p} = \boldsymbol{F}^{\mathrm{p}} \tag{2}$$

where $\boldsymbol{M}$, $\boldsymbol{Q}$, $\boldsymbol{K}$, $\boldsymbol{S}$, and $\boldsymbol{H}$ denote the mass matrix, the coupling matrix, the stiffness matrix, the compression matrix of the fluid, and the flow matrix of the fluid, respectively; $\boldsymbol{F}^{\mathrm{u}}$ and $\boldsymbol{F}^{\mathrm{p}}$ are the load vectors applied to the soil skeleton and the fluid, respectively; $\boldsymbol{u}$ and $\boldsymbol{p}$ are the displacement and pore fluid pressure vectors, respectively; and the dot stands for the derivatives with respect to the time.

Express Equations (1) and (2) separately for the interior domain Ω^- and the exterior domain Ω^+ as:

$$\begin{bmatrix} \boldsymbol{M}_{\mathrm{ii}}^{\Omega^-} & \boldsymbol{M}_{\mathrm{ib}}^{\Omega^-} \\ \boldsymbol{M}_{\mathrm{bi}}^{\Omega^-} & \boldsymbol{M}_{\mathrm{bb}}^{\Omega^-} \end{bmatrix} \begin{bmatrix} \ddot{\boldsymbol{u}}_{\mathrm{i}} \\ \ddot{\boldsymbol{u}}_{\mathrm{b}} \end{bmatrix} - \begin{bmatrix} \boldsymbol{Q}_{\mathrm{ii}}^{\Omega^-} & \boldsymbol{Q}_{\mathrm{ib}}^{\Omega^-} \\ \boldsymbol{Q}_{\mathrm{bi}}^{\Omega^-} & \boldsymbol{Q}_{\mathrm{bb}}^{\Omega^-} \end{bmatrix} \begin{bmatrix} \boldsymbol{p}_{\mathrm{i}} \\ \boldsymbol{p}_{\mathrm{b}} \end{bmatrix} + \begin{bmatrix} \boldsymbol{K}_{\mathrm{ii}}^{\Omega^-} & \boldsymbol{K}_{\mathrm{ib}}^{\Omega^-} \\ \boldsymbol{K}_{\mathrm{bi}}^{\Omega^-} & \boldsymbol{K}_{\mathrm{bb}}^{\Omega^-} \end{bmatrix} \begin{bmatrix} \boldsymbol{u}_{\mathrm{i}} \\ \boldsymbol{u}_{\mathrm{b}} \end{bmatrix} = \begin{bmatrix} 0 \\ \boldsymbol{F}_{\mathrm{b}}^{\mathrm{u}} \end{bmatrix} \text{ in } \Omega^- \tag{3}$$

$$\begin{bmatrix} \boldsymbol{M}_{\mathrm{bb}}^{\Omega^+} & \boldsymbol{M}_{\mathrm{be}}^{\Omega^+} \\ \boldsymbol{M}_{\mathrm{eb}}^{\Omega^+} & \boldsymbol{M}_{\mathrm{ee}}^{\Omega^+} \end{bmatrix} \begin{bmatrix} \ddot{\boldsymbol{u}}_{\mathrm{b}} \\ \ddot{\boldsymbol{u}}_{\mathrm{e}} \end{bmatrix} - \begin{bmatrix} \boldsymbol{Q}_{\mathrm{bb}}^{\Omega^+} & \boldsymbol{Q}_{\mathrm{be}}^{\Omega^+} \\ \boldsymbol{Q}_{\mathrm{eb}}^{\Omega^+} & \boldsymbol{Q}_{\mathrm{ee}}^{\Omega^+} \end{bmatrix} \begin{bmatrix} \boldsymbol{p}_{\mathrm{b}} \\ \boldsymbol{p}_{\mathrm{e}} \end{bmatrix} + \begin{bmatrix} \boldsymbol{K}_{\mathrm{bb}}^{\Omega^+} & \boldsymbol{K}_{\mathrm{be}}^{\Omega^+} \\ \boldsymbol{K}_{\mathrm{eb}}^{\Omega^+} & \boldsymbol{K}_{\mathrm{ee}}^{\Omega^+} \end{bmatrix} \begin{bmatrix} \boldsymbol{u}_{\mathrm{b}} \\ \boldsymbol{u}_{\mathrm{e}} \end{bmatrix} = \begin{bmatrix} -\boldsymbol{F}_{\mathrm{b}}^{\mathrm{u}} \\ \boldsymbol{F}_{\mathrm{e}}^{\mathrm{u}} \end{bmatrix} \text{ in } \Omega^+ \tag{4}$$

$$\begin{bmatrix} \boldsymbol{S}_{\mathrm{ii}}^{\Omega^-} & \boldsymbol{S}_{\mathrm{ib}}^{\Omega^-} \\ \boldsymbol{S}_{\mathrm{bi}}^{\Omega^-} & \boldsymbol{S}_{\mathrm{bb}}^{\Omega^-} \end{bmatrix} \begin{bmatrix} \dot{\boldsymbol{p}}_{\mathrm{i}} \\ \dot{\boldsymbol{p}}_{\mathrm{b}} \end{bmatrix} + \begin{bmatrix} (\boldsymbol{Q}_{\mathrm{ii}}^{\Omega^-})^{\mathrm{T}} & (\boldsymbol{Q}_{\mathrm{ib}}^{\Omega^-})^{\mathrm{T}} \\ (\boldsymbol{Q}_{\mathrm{bi}}^{\Omega^-})^{\mathrm{T}} & (\boldsymbol{Q}_{\mathrm{bb}}^{\Omega^-})^{\mathrm{T}} \end{bmatrix} \begin{bmatrix} \dot{\boldsymbol{u}}_{\mathrm{i}} \\ \dot{\boldsymbol{u}}_{\mathrm{b}} \end{bmatrix} + \begin{bmatrix} \boldsymbol{H}_{\mathrm{ii}}^{\Omega^-} & \boldsymbol{H}_{\mathrm{ib}}^{\Omega^-} \\ \boldsymbol{H}_{\mathrm{bi}}^{\Omega^-} & \boldsymbol{H}_{\mathrm{bb}}^{\Omega^-} \end{bmatrix} \begin{bmatrix} \boldsymbol{p}_{\mathrm{i}} \\ \boldsymbol{p}_{\mathrm{b}} \end{bmatrix} = \begin{bmatrix} 0 \\ \boldsymbol{F}_{\mathrm{b}}^{\mathrm{p}} \end{bmatrix} \text{ in } \Omega^- \tag{5}$$

$$\begin{bmatrix} \boldsymbol{S}_{\mathrm{bb}}^{\Omega^+} & \boldsymbol{S}_{\mathrm{be}}^{\Omega^+} \\ \boldsymbol{S}_{\mathrm{eb}}^{\Omega^+} & \boldsymbol{S}_{\mathrm{ee}}^{\Omega^+} \end{bmatrix} \begin{bmatrix} \dot{\boldsymbol{p}}_{\mathrm{b}} \\ \dot{\boldsymbol{p}}_{\mathrm{e}} \end{bmatrix} + \begin{bmatrix} (\boldsymbol{Q}_{\mathrm{bb}}^{\Omega^+})^{\mathrm{T}} & (\boldsymbol{Q}_{\mathrm{be}}^{\Omega^+})^{\mathrm{T}} \\ (\boldsymbol{Q}_{\mathrm{eb}}^{\Omega^+})^{\mathrm{T}} & (\boldsymbol{Q}_{\mathrm{ee}}^{\Omega^+})^{\mathrm{T}} \end{bmatrix} \begin{bmatrix} \dot{\boldsymbol{u}}_{\mathrm{b}} \\ \dot{\boldsymbol{u}}_{\mathrm{e}} \end{bmatrix} + \begin{bmatrix} \boldsymbol{H}_{\mathrm{bb}}^{\Omega^+} & \boldsymbol{H}_{\mathrm{be}}^{\Omega^+} \\ \boldsymbol{H}_{\mathrm{eb}}^{\Omega^+} & \boldsymbol{H}_{\mathrm{ee}}^{\Omega^+} \end{bmatrix} \begin{bmatrix} \boldsymbol{p}_{\mathrm{b}} \\ \boldsymbol{p}_{\mathrm{e}} \end{bmatrix} = \begin{bmatrix} -\boldsymbol{F}_{\mathrm{b}}^{\mathrm{p}} \\ \boldsymbol{F}_{\mathrm{e}}^{\mathrm{p}} \end{bmatrix} \text{ in } \Omega \tag{6}$$

where the subscripts *i*, *b* and *e* refer to elements or nodes in the interior domain, on the boundary Γ and in the exterior domain, respectively.

With the assumption that the exterior domain is linear-elastic, its dynamic response can be readily written as the superposition of free and residual components:

$$\boldsymbol{u}_{\mathrm{e}} = \boldsymbol{u}_{\mathrm{e}}^{\mathrm{f}} + \boldsymbol{u}_{\mathrm{e}}^{\mathrm{w}} \tag{7}$$

$$\boldsymbol{p}_{\mathrm{e}} = \boldsymbol{p}_{\mathrm{e}}^{\mathrm{f}} + \boldsymbol{p}_{\mathrm{e}}^{\mathrm{w}} \tag{8}$$

where $\boldsymbol{u}_{\mathrm{e}}^{\mathrm{w}}$ and $\boldsymbol{p}_{\mathrm{e}}^{\mathrm{w}}$ denote the difference of the ground responses in the exterior ground with respect to the free field responses $\boldsymbol{u}_{\mathrm{e}}^{\mathrm{f}}$ and $\boldsymbol{p}_{\mathrm{e}}^{\mathrm{f}}$. Substitution of Equations (7) and (8) into (3) and (4) gives:

$$\begin{aligned} &\begin{bmatrix} \boldsymbol{M}_{\mathrm{ii}}^{\Omega^-} & \boldsymbol{M}_{\mathrm{ib}}^{\Omega^-} & 0 \\ \boldsymbol{M}_{\mathrm{bi}}^{\Omega^-} & \boldsymbol{M}_{\mathrm{bb}}^{\Omega^-} + \boldsymbol{M}_{\mathrm{bb}}^{\Omega^+} & \boldsymbol{M}_{\mathrm{be}}^{\Omega^+} \\ 0 & \boldsymbol{M}_{\mathrm{eb}}^{\Omega^+} & \boldsymbol{M}_{\mathrm{ee}}^{\Omega^+} \end{bmatrix} \begin{bmatrix} \ddot{\boldsymbol{u}}_{\mathrm{i}} \\ \ddot{\boldsymbol{u}}_{\mathrm{b}} \\ \ddot{\boldsymbol{u}}_{\mathrm{e}}^{\mathrm{w}} \end{bmatrix} - \begin{bmatrix} \boldsymbol{Q}_{\mathrm{ii}}^{\Omega^-} & \boldsymbol{Q}_{\mathrm{ib}}^{\Omega^-} & 0 \\ \boldsymbol{Q}_{\mathrm{bi}}^{\Omega^-} & \boldsymbol{Q}_{\mathrm{bb}}^{\Omega^-} + \boldsymbol{Q}_{\mathrm{bb}}^{\Omega^+} & \boldsymbol{Q}_{\mathrm{be}}^{\Omega^+} \\ 0 & \boldsymbol{Q}_{\mathrm{eb}}^{\Omega^+} & \boldsymbol{Q}_{\mathrm{ee}}^{\Omega^+} \end{bmatrix} \begin{bmatrix} \boldsymbol{p}_{\mathrm{i}} \\ \boldsymbol{p}_{\mathrm{b}} \\ \boldsymbol{p}_{\mathrm{e}}^{\mathrm{w}} \end{bmatrix} \\ &+ \begin{bmatrix} \boldsymbol{K}_{\mathrm{ii}}^{\Omega^-} & \boldsymbol{K}_{\mathrm{ib}}^{\Omega^-} & 0 \\ \boldsymbol{K}_{\mathrm{bi}}^{\Omega^-} & \boldsymbol{K}_{\mathrm{bb}}^{\Omega^-} + \boldsymbol{K}_{\mathrm{bb}}^{\Omega^+} & \boldsymbol{K}_{\mathrm{be}}^{\Omega^+} \\ 0 & \boldsymbol{K}_{\mathrm{eb}}^{\Omega^+} & \boldsymbol{K}_{\mathrm{ee}}^{\Omega^+} \end{bmatrix} \begin{bmatrix} \boldsymbol{u}_{\mathrm{i}} \\ \boldsymbol{u}_{\mathrm{b}} \\ \boldsymbol{u}_{\mathrm{e}}^{\mathrm{w}} \end{bmatrix} = \begin{bmatrix} 0 \\ -\boldsymbol{M}_{\mathrm{be}}^{\Omega^+} \ddot{\boldsymbol{u}}_{\mathrm{e}}^{\mathrm{f}} + \boldsymbol{Q}_{\mathrm{be}}^{\Omega^+} \boldsymbol{p}_{\mathrm{e}}^{\mathrm{f}} - \boldsymbol{K}_{\mathrm{be}}^{\Omega^+} \boldsymbol{u}_{\mathrm{e}}^{\mathrm{f}} \\ \boldsymbol{M}_{\mathrm{eb}}^{\Omega^+} \ddot{\boldsymbol{u}}_{\mathrm{b}}^{\mathrm{f}} - \boldsymbol{Q}_{\mathrm{eb}}^{\Omega^+} \boldsymbol{p}_{\mathrm{b}}^{\mathrm{f}} + \boldsymbol{K}_{\mathrm{eb}}^{\Omega^+} \boldsymbol{u}_{\mathrm{b}}^{\mathrm{f}} \end{bmatrix} \end{aligned} \tag{9}$$

Since the unknown variables on the left side of Equation (9) are identical to those of Equations (3) and (4), it is evident that the seismic excitation outside the interior domain can be replaced by the equivalent nodal forces applied on the boundaries Γ and Γ_e:

$$\begin{bmatrix} \boldsymbol{F}_{\mathrm{b,eff}}^{\mathrm{u}} \\ \boldsymbol{F}_{\mathrm{e.eff}}^{\mathrm{u}} \end{bmatrix} = \begin{bmatrix} -\boldsymbol{M}_{\mathrm{be}}^{\Omega^+} \ddot{\boldsymbol{u}}_{\mathrm{e}}^{\mathrm{f}} + \boldsymbol{Q}_{\mathrm{be}}^{\Omega^+} \boldsymbol{p}_{\mathrm{e}}^{\mathrm{f}} - \boldsymbol{K}_{\mathrm{be}}^{\Omega^+} \boldsymbol{u}_{\mathrm{e}}^{\mathrm{f}} \\ \boldsymbol{M}_{\mathrm{eb}}^{\Omega^+} \ddot{\boldsymbol{u}}_{\mathrm{b}}^{\mathrm{f}} - \boldsymbol{Q}_{\mathrm{eb}}^{\Omega^+} \boldsymbol{p}_{\mathrm{b}}^{\mathrm{f}} + \boldsymbol{K}_{\mathrm{eb}}^{\Omega^+} \boldsymbol{u}_{\mathrm{b}}^{\mathrm{f}} \end{bmatrix} \tag{10}$$

Likewise, the equivalent nodal forces acting on the fluid phase can be obtained as:

$$\begin{bmatrix} \boldsymbol{F}_{\mathrm{b,eff}}^{\mathrm{p}} \\ \boldsymbol{F}_{\mathrm{e,eff}}^{\mathrm{p}} \end{bmatrix} = \begin{bmatrix} -\boldsymbol{S}_{\mathrm{be}}^{\Omega^+}\, \dot{\boldsymbol{p}}_{\mathrm{e}}^{\,\mathrm{f}} - (\boldsymbol{Q}_{\mathrm{be}}^{\Omega^+})^{\mathrm{T}} \dot{\boldsymbol{u}}_{\mathrm{e}}^{\,\mathrm{f}} - \boldsymbol{H}_{\mathrm{be}}^{\Omega^+}\, \boldsymbol{p}_{\mathrm{e}}^{\,\mathrm{f}} \\ \boldsymbol{S}_{\mathrm{eb}}^{\Omega^+}\, \dot{\boldsymbol{p}}_{\mathrm{b}}^{\,\mathrm{f}} + (\boldsymbol{Q}_{\mathrm{eb}}^{\Omega^+})^{\mathrm{T}} \dot{\boldsymbol{u}}_{\mathrm{b}}^{\,\mathrm{f}} + \boldsymbol{H}_{\mathrm{eb}}^{\Omega^+}\, \boldsymbol{p}_{\mathrm{b}}^{\,\mathrm{f}} \end{bmatrix} \tag{11}$$

In Equations (10) and (11), the nodal forces are dependent on the free-field responses, the locations, and the material parameters of the elements enclosed by the boundaries Γ and Γ_e. Notably, these forces are independent of the material and geometric properties of the interior domain, which is why the domain reduction method (DRM) is particularly advantageous for complex interior domains. It should also be mentioned that the free field responses at DRM boundaries need to be determined beforehand. To calculate these responses in our study, an analytical approach proposed for layered saturated grounds is utilized [14].

3 Parametric studies

3.1 Model configurations

The numerical simulations presented in this study were conducted using Opensees, a widely used open-source finite element platform [15]. The model layout is depicted in Figure 2, where twin tunnels are constructed at the interface level of two neighboring soil layers, with thicknesses of 25m and 75m, respectively.

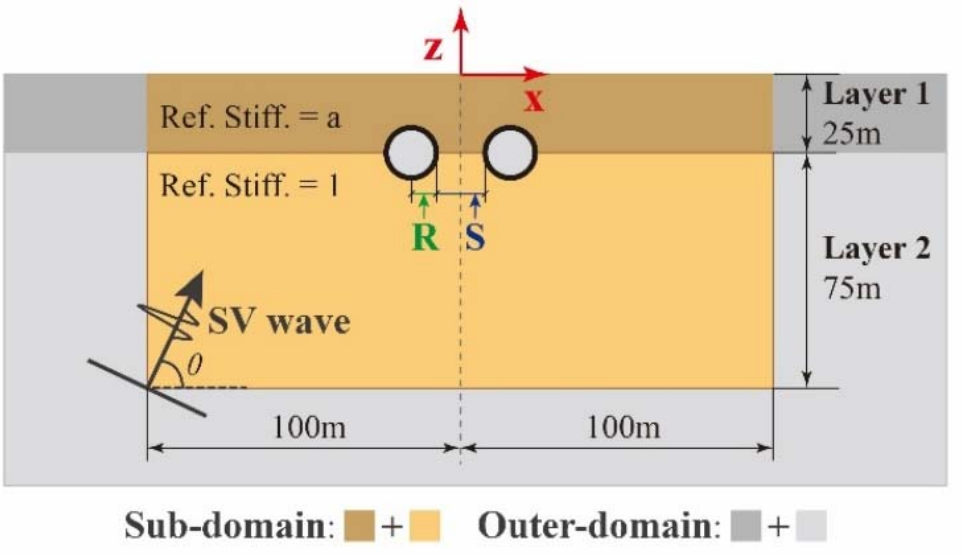

Figure 2: Illustrations of the numerical model

The soil skeleton is modeled using an advanced constitutive model known as the *Pressure-Dependent-Multi-Yield (PDMY02)* soil model, which assumes elastoplastic behavior. The soil parameters used in the simulations are listed in Table 1. The only

distinguishing factor between the two soil layers is the reference elastic modulus. To investigate the effects of this parameter, we varied the stiffness ratio a, which represents the ratio of the reference elastic modulus of Layer 1 to that of Layer 2, in the following parametric analysis.

	Layer 1	**Layer 2**
Mixture density (ton/m^3)	1.99	1.99
Reference shear modulus (kPa)	a*9.6e4	9.6e4
Reference bulk modulus(kPa)	a*20.8e4	20.8e4
Friction angle (°)	33.5	33.5
Phase transform angle (°)	25.5	25.5
Peak shear strain	0.1	0.1
Reference pressure (kPa)	101	101
Pressure dependent coefficient	0.0	0.0
Contraction coefficient 1	0.045	0.045
Contraction coefficient 3	0.15	0.15
Dilation coefficient 1	0.06	0.06
Dilation coefficient 3	0.15	0.15
Void ratio	0.67	0.67
Fluid compressibility (kPa)	2.2e6	2.2e6
Permeability (m/s)	1e-4	1e-4

Table 1: Soil parameters

The twin tunnels are meshed using the Force-Based Beam-Column element with a fiber section, and the material behaviors of concrete and rebars are modeled by *Concrete01* and *Steel01*, respectively. Table 2 summarizes the structural parameters. The ratio of spacing to radius of the twin tunnels, is the second factor analyzed in the parametric analysis.

Geometry	Diameter (m)	16
	Thickness (m)	0.7
	Reinforce ratio	0.4%
Concrete	Strength at 28 days (kPa)	-34474.8
	Strain at maximum strength	-0.005
	Crushing strength (kPa)	-24131.7
	Strain at crushing strength	-0.02
Rebar	Yield strength (kPa)	248200
	Initial elastic tangent (kPa)	2.1e8
	Strain-hardening ratio	0.02

Table 2: Structural parameters

In this study, only SV wave is considered as the seismic input, and the incidence angle is chosen as the third influencing factor. A Ricker wavelet with a central

frequency of 3Hz and an amplitude of 0.002m is used for all simulations, as shown in Figure 3.

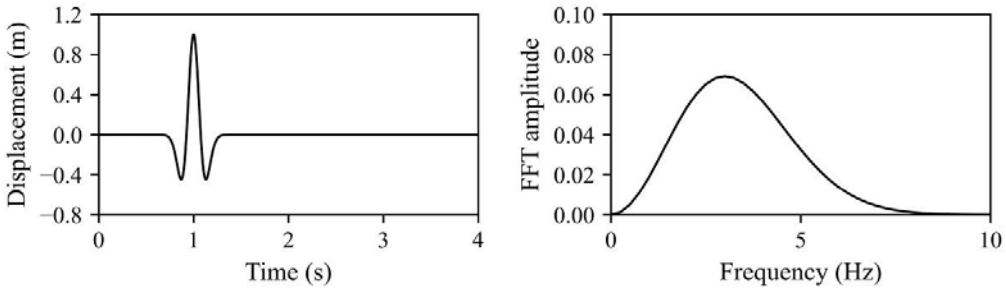

Figure 3: The input Ricker wavelet

3.2 Results and Discussions

In Opensees, the *PDMY02* model provides a convenient means for users to switch between elastic and elastoplastic material stages using the *updateMaterialStage* command. The Lame constants employed in the elastic mode are derived from the reference shear and bulk modulus values presented in Table 1. This results in the elastic and elastoplastic modes being equivalent until the stress path reaches the initial yield surface, as shown in Figures 4a and 4b. However, when the incident wave encounters the ground surface or twin tunnels, the elastic field exhibits smaller responses, as illustrated in Figures 4c and 4d. As the reflection waves leave the calculation regions, permanent displacement can only be observed in the elastoplastic subdomain, as shown in Figures 4e and 4f. It is important to note that in this study, the calculation domain is assumed to be elastoplastic, incorporating pore water pressure accumulation and accumulative deformations during cyclic loadings.

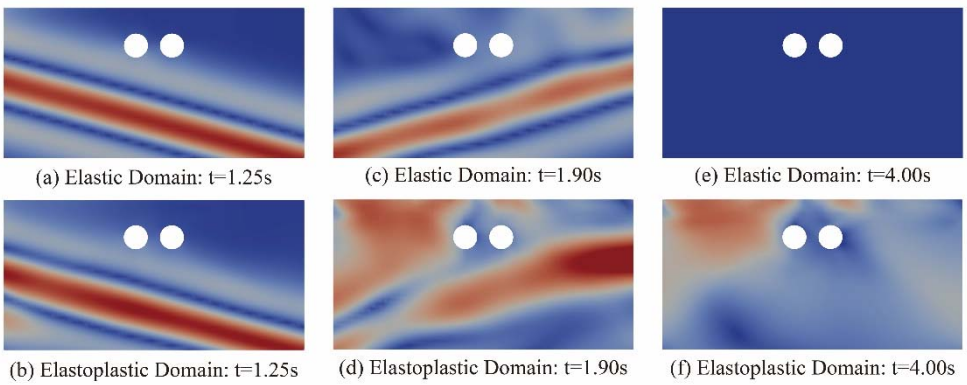

Figure 4: Displacement contours of subdomains (left: elastic, right: elastoplastic) when a=1.0, S/R=1.0, and θ=75°.

Figure 5 presents an analysis of the influence of soil stiffness ratio, with an angle of incidence of 75° and a spacing-radius ratio of 1.0 for all cases. The results show that the stiffness ratio has a notable impact on the moment of the tunnel linings.

Specifically, the maximum moment increases monotonically with higher stiffness of the upper soil layer. However, this amplification of internal forces due to larger soil stiffness discontinuity is less significant in terms of the shear and axial forces.

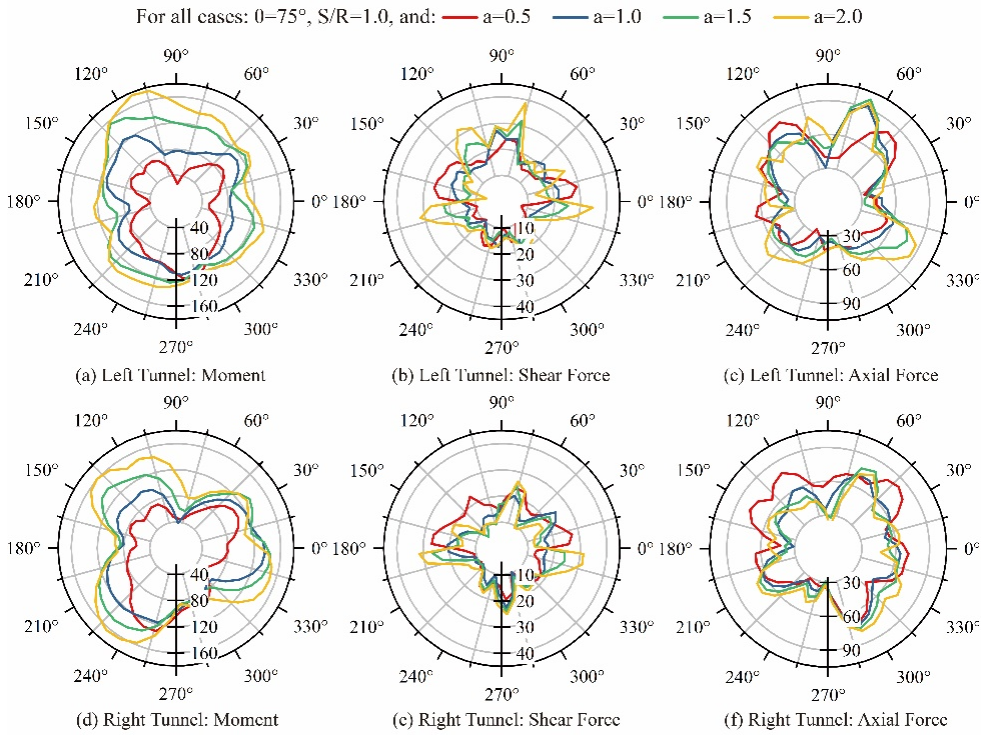

Figure 5: Comparisons of internal force responses with various soil stiffness ratios

In Figure 6, the influence of tunnel spacings is investigated. The findings reveal that, in terms of the lining moments, the magnitude exhibits only slight variation with increasing S/R values. However, a noticeable change in the direction of the principle axis (i.e., the direction of the maximum internal force) is observed, with different distribution patterns observed for the left and right tunnels. The distribution patterns for the shear and axial forces, on the other hand, remain similar with larger tunnel spacings but exhibit increasing magnitudes.

Figure 7 displays the maximum internal force responses of the shield tunnel at varying incident angles θ. As observed, the distributions of both moments and axial forces are markedly impacted by the incident angle, with a 45-degree angle existing between the principle axis and the incident direction. For comparison, the distribution patterns of the shear force exhibit minor variations across the range of θ values. Although the distribution patterns of the two tunnels evolve similarly, some differences are present. For instance, the left tunnel experiences the highest shear force magnitude at θ=60°, whereas the maximum value for the right tunnel occurs at θ=90°.

Given the length limitation of this paper, the parametric analysis presented above remains preliminary. For the sake of simplicity, the Ricker wavelet has been chosen as the input motion, limiting the observation of more complex behaviors, such as

cyclic mobility in saturated sands under long-time cyclic excitation. Additionally, the analysis has only considered a limited range of parameter choices, hindering the ability to draw more general conclusions. Therefore, more in-depth parametric analysis is still necessary to be carried out in the future.

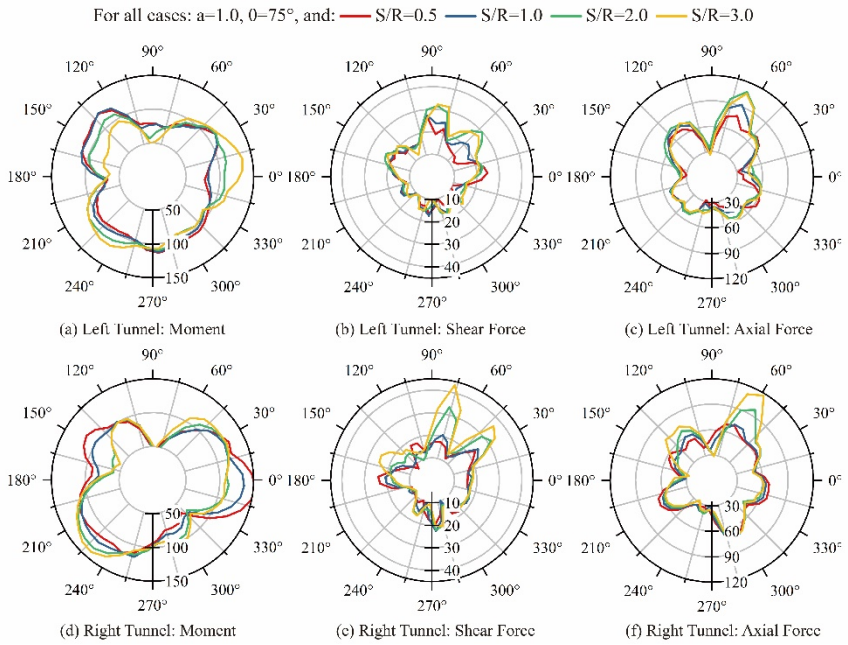

Figure 6: Comparisons of internal force responses with various spacings

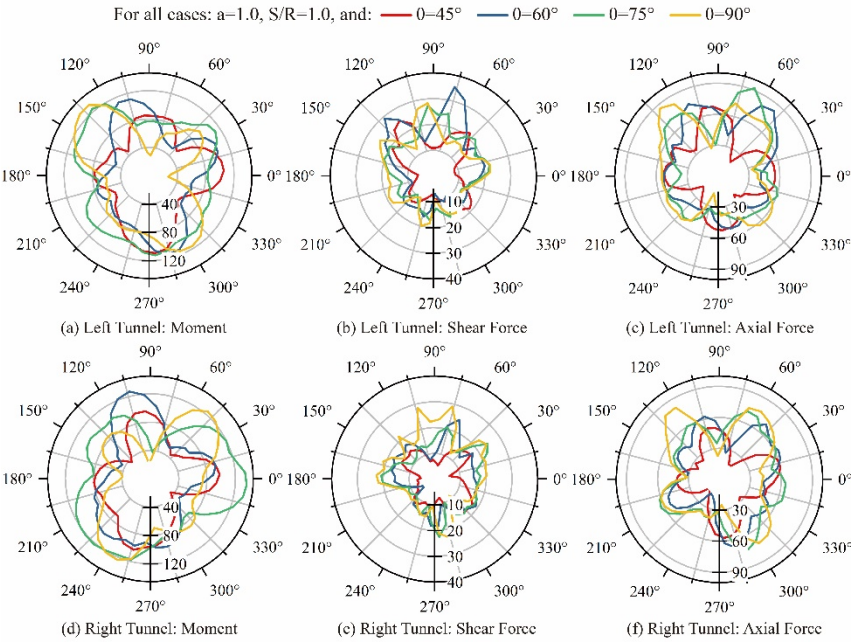

Figure 7: Comparisons of internal force responses with various incidence angle

4 Conclusions and Contributions

During earthquakes, underground structures located in saturated liquefiable fields are vulnerable to damage due to seismic-induced liquefaction. This paper investigates the dynamic behavior of a pair of twin tunnels constructed at the interface of neighboring soil layers, with a primary focus on the structural internal forces. To accurately analyze complex soil-structure interaction (SSI) problems, a DRM-based scheme is extended to layered saturated grounds to better replicate the incident seismic wavefields. The results reveal that the stiffness ratio between soil layers, the spacing-radius ratio of tunnels, and the angle of incidence of seismic inputs significantly influence the dynamic responses of the twin-tunnel system. Specifically, the magnitude of internal force responses increases with a higher soil stiffness ratio, while directionality varies with the angle of seismic incidence. Tunnel spacing affects both magnitude and directionality, but to a lesser extent. The proposed DRM-based scheme can provide accurate analysis of SSI problems, enabling better prediction of the dynamic behavior of twin-tunnel systems and improved design of underground structures in liquefiable soils.

Acknowledgements

The research is supported by the National Natural Science Foundation of China (with grant No. 51778487).

References

[1] M. Hamada, R. Isoyama, and K. Wakamatsu, "Liquefaction-induced ground displacement and its related damage to lifeline facilities," *Soils Found.*, no. Special, pp. 81–97, 1996, doi: 10.3208/sandf.36.special_81.

[2] F. Yue, B. Liu, B. Zhu, X. Jiang, L. Chen, and K. Liao, "Shaking table test and numerical simulation on seismic performance of prefabricated corrugated steel utility tunnels on liquefiable ground," *Soil Dyn. Earthq. Eng.*, vol. 141, no. March 2020, p. 106527, 2021, doi: 10.1016/j.soildyn.2020.106527.

[3] Y. Yang, S. Zhang, J. Zhang, Y. Yuan, and H. Yu, "Analytical solution for long tunnels in layered saturated poroelastic ground under inclined P1-SV waves," *Tunn. Undergr. Sp. Technol.*, vol. 124, p. 104458, 2022, doi: 10.1016/j.tust.2022.104458.

[4] X. Bao, Z. Xia, G. Ye, Y. Fu, and D. Su, "Numerical analysis on the seismic behavior of a large metro subway tunnel in liquefiable ground," *Tunn. Undergr. Sp. Technol.*, vol. 66, no. March, pp. 91–106, 2017, doi: 10.1016/j.tust.2017.04.005.

[5] H. Liu, "Three-dimensional analysis of underground tunnels in liquefiable soil subject to earthquake loading," in *GeoCongress 2012: State of the Art and Practice in Geotechnical Engineering*, 2012, pp. 1819–1828.

[6] B. Unutmaz, "Liquefaction potential of soils around circular double tunnels," *Bull. Earthq. Eng.*, vol. 14, no. 2, pp. 391–411, 2016, doi: 10.1007/s10518-015-9831-1.

[7] G. Zheng, P. Yang, H. Zhou, W. Zhang, T. Zhang, and S. Ma, “Numerical Modeling of the Seismically Induced Uplift Behavior of Twin Tunnels,” *Int. J. Geomech.*, vol. 21, no. 1, pp. 1–12, 2021, doi: 10.1061/(asce)gm.1943-5622.0001897.

[8] B. Sun, M. Deng, S. Zhang, C. Wei, C, Wang, L. Yu, and K. Cao, “Inelastic dynamic analysis and damage assessment of a hydraulic arched tunnel under near-fault SV waves with arbitrary incoming angles,” *Tunn. Undergr. Sp. Technol.*, vol. 104, p. 103523, 2020, doi: 10.1016/j.tust.2020.103523.

[9] J. Bielak, K. Loukakis, Y. Hisada, and C. Yoshimura, “Domain reduction method for three-dimensional earthquake modeling in localized regions, Part I: Theory,” *Bull. Seismol. Soc. Am.*, vol. 93, no. 2, pp. 817–824, 2003.

[10] B. Jeremić, N. Tafazzoli, T. Ancheta, N. Orbović, and A. Blahoianu, “Seismic behavior of NPP structures subjected to realistic 3D, inclined seismic motions, in variable layered soil/rock, on surface or embedded foundations,” *Nucl. Eng. Des.*, vol. 265, pp. 85–94, 2013, doi: 10.1016/j.nucengdes.2013.07.003.

[11] S. Kontoe, L. Zdravkovic, C. O. Menkiti, and D. M. Potts, “Seismic response and interaction of complex soil retaining systems,” *Comput. Geotech.*, vol. 39, pp. 17–26, 2012, doi: 10.1016/j.compgeo.2011.08.003.

[12] W. Zhang, *A Quantitative Seismic Behavior Assessment of Buried Structures*. University of California, Los Angeles, 2019.

[13] O. C. Zienkiewicz and T. Shiomi, “Dynamic behaviour of saturated porous media; The generalized Biot formulation and its numerical solution,” *Int. J. Numer. Anal. Methods Geomech.*, vol. 8, no. 1, pp. 71–96, 1984, doi: 10.1002/nag.1610080106.

[14] J. Liang and H. You, “Dynamic stiffness matrix of a poroelastic multi-layered site and its Green’s functions,” *Earthq. Eng. Eng. Vib.*, vol. 3, no. 2, pp. 273–282, 2004, doi: 10.1007/bf02858241.

[15] S. Mazzoni, F. McKenna, M. H. Scott, and G. L. Fenves, “OpenSees command language manual,” *Pacific Earthq. Eng. Res. Cent.*, vol. 264, pp. 137–158, 2006.